Influence of machining parameters on fretting fatigue life of Inconel 718.

D. Infante-García[1], A. Díaz-Álvarez[1], J.L. Cantero[1], R. Belda[2], J. Díaz-Álvarez[1], E. Giner[2] and H. Miguélez[1].

[(1)] Dept. of Mechanical Engineering, University Carlos III of Madrid, Avda. de la Universidad 30, 28911 Leganes, Madrid, Spain.

[(2)] Centre of Research in Mechanical Engineering - CIIM, Dept. of Mechanical Engineering and Materials, Universitat Politècnica de València, Camino de Vera, 46022 Valencia, Spain.

**Corresponding author: dinfante@ing.uc3m.es*

Abstract

This work focuses on the analysis of the influence of different machining factors on the fretting fatigue behaviour of Inconel 718. In this way, fretting fatigue tests using a flat-to-flat with rounded edges are carried out with specimens machined using different manufacturing process parameters such as tool state, cutting tool, cutting speed and coolant pressure. In addition, surface integrity, in terms of surface roughness and surface residual stresses, is characterized for all machining conditions in two orthogonal directions. The results pointed out the high impact that machining process parameters possess in hard-to-cut materials such as Inconel 718 in their fretting fatigue lifetime. Tool wear has been shown to be the most significant parameter affecting the fretting fatigue lifetime and surface integrity. Lastly, residual stresses measured along the direction of fatigue load have proved to be a relevant indicator of the fretting fatigue behaviour. On the other hand, surface roughness has been shown to possess a weaker influence.

KEYWORDS. Fretting fatigue, Machining parameters, Inconel 718

Graphical Abstract

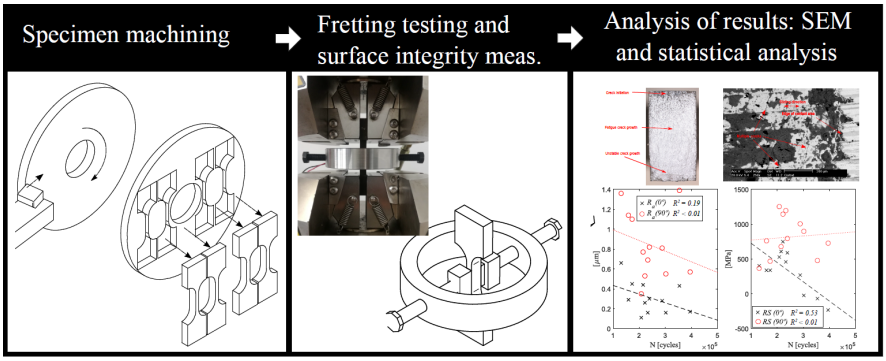

1. Introduction

Nickel-based alloys are widely used in critical parts for turbine engines, such as blades or disks, due to their excellent fatigue strength and corrosive resistance at high temperatures [1]. Furthermore, these relevant mechanical properties at high temperatures involve characteristic low machinability of nickel-based alloys Inconel 718 is the most used alloy in this family, for instance, 34% of the total weight in a CF6 engine of General Electric was Inconel 718 [2].

Surface integrity (SI) of critical components is crucial to ensure proper in-service behaviour. The high mechanical and thermal loads developed during machining Inconel 718 may change the mechanical behaviour of the material located at the machined surface and near sub-surface in comparison to the bulk material. In this way, plastic deformation, phase transformations, notches, microcracks or residual stresses can be found after machining [3]. Due to its high industrial significance, it can be found extensive Inconel 718 literature regarding the effect of machining on SI and fatigue behaviour [4–9]. However, although fretting fatigue has been commonly responsible for the failure at the blade and disk attachment or at bolt holes of disks [10,11], there is a lack of researching works analysing the machining effect on the fretting fatigue behaviour of Inconel 718.

Fretting involves some minute oscillatory displacement between two solids in contact [12]. When the amplitude of the relative oscillatory movement is very small (30microns), fretting results in the rapid initiation of cracks and some material removal between the two contacting surfaces, commonly named as fretting debris. As stated by Szolwinski and Farris [13], fretting fatigue is a synergistic competition between multiple phenomena such as fatigue, wear and corrosion. In fretting fatigue, cracks are usually initiated at the edge of the contact pair on the surface. Contact conditions and surface state of the solids become relevant factors in their tolerance to fretting damage. Therefore, the SI of the final components is a significant factor influencing fretting behaviour. In fact, surface modifications, such as surface chemical treatments (phosphating, anodizing and sulphidizing), surface mechanical treatments (shot or wet peening, etc…), metal or non-metallic coatings and, recently, surface texturing are commonly used as palliatives to fretting fatigue [14]. It is noted in [14] that some of the relevant parameters (friction, slip, pressure, etc..) affecting fretting fatigue are interactive linked. Therefore, palliatives must be specifically applied to each fretting fatigue problem and not in a general way.

Regarding the influence of the topography in fretting fatigue, Waterhouse et al. [15] observed that roughness introduced by shot-peening was less damaging in fretting fatigue as in plain fatigue. They conclude that a specimen with higher roughness presents smaller real contact area, thus the critical volume of material per contact to initiate a crack is not achieved as proposed by Bramhall [16]. A

similar result was recently found by Martin et al. [17] when testing specimens polished and untouched after shot-peening under fretting fatigue conditions. The authors did not see a significant improvement between the samples polished and as-received. Vazquez et al. [18] observed similar results when polishing specimens of an aluminium alloy after shot-peening. The polished after shot-peening specimens reached a smaller number of cycles until fretting fatigue fracture than the shot-peening specimens. However, when comparing surfaces with a better surface finish, Taketa et al. [19] observed that smoother polished surfaces increase the fretting fatigue strength up to a 20% in a titanium alloy. In addition, Proutdhon et al. [20] investigated the influence of the unidirectional roughness obtained by machining at high speed, low speed and polishing in fretting crack initiation. They observed that a smoother surface leads to a higher value of the tangential force needed for crack initiation. Hutson et al. [21] investigated the fretting fatigue behaviour of a titanium alloy specimen in contact with different pad surface conditions. The Cu-Ni coating and the polished specimen showed a significant improvement of the fretting fatigue strength in comparison to the alloy tested against itself as received. The main cause of the improvement resulted from the decrease of the surface roughness rather than from the contact material. On the other hand, introduction of surface regular micro topography can double the fretting fatigue strength as pointed out in [22]. In general, it has been observed different trends of the influence of SI in fretting fatigue compared to observations in plain fatigue.

In reference to the influence of the residual stress induced by surface treatments, Li et al. [23] investigated the fretting fatigue behaviour of a titanium alloy after wet peening treatment. The wet peening specimens showed higher fretting fatigue resistance due to the layer of compressive residual stress. Liu et al. [24] studied the effect of different coatings in combination with shot peening on fretting fatigue resistance. Coatings and shot peening improved the fretting fatigue resistance depending on the sliding contact conditions. A similar conclusion was achieved by Chakravarty et al. [25]. They did not find any improvement of the fretting fatigue resistance of different ion implantation when compared with the shot-peening treatment. Zhang and Liu [26] investigated the effect of shot peening on the fretting fatigue resistance at elevated temperature of a titanium alloy. They found that compressive residual stress is the relevant parameter in the improvement of the fretting fatigue resistance. Furthermore, surface roughness was detrimental to the fretting fatigue resistance at elevated temperatures. Lastly, Murthy et al. [27] tested different surface treatments on a titanium alloy specimen under uniaxial, multiaxial and fretting fatigue tests. Coatings and shot peening showed a similar increment in the fretting fatigue strength as compared with plain fatigue tests. In addition, propagation was more significant in the total life on fretting fatigue tests than on uniaxial or multiaxial fatigue tests.

Little information can be found about the influence of the SI on the fretting fatigue resistance of nickel-based alloys. Few papers can be found in the literature regarding the improvement of fretting fatigue resistance due to the introduction of compressive residual stresses using shot-peening [28,29]. Some works can be found in the literature regarding the fretting fatigue behaviour of alloys belonging to the Inconel series [30–34] [201–206]. Under plain fatigue conditions, Kawagoishi et al. [35] investigated the fatigue strength of Inconel 718 solution treated and aged at high and room temperatures. They observed an increase of fatigue strength at high temperatures in the long-life region as a result of the creation of oxide films and induced plasticity. Wang et al. [9] investigated the changes on the fatigue life of Inconel 718 specimens machined with different feed rates and cutting speeds using a milling machine. They observed significant influence of the feed rate, but no effect of cutting speed when machining with carbide inserts. The improvement of the fatigue strength under plain fatigue conditions at high temperature is also observed under fretting fatigue conditions. Waterhouse [34] found that the strength reduction factor was 2.29 at room temperature and 1.29 at 540◦C. They pointed out that the formation of glaze oxide in the fretted region at high temperatures acted as a protective coating. The improvement of the fretting fatigue strength at high temperatures is also observed in nickel-based alloys belonging to the family of Inconel alloys. For instance, Mall et al. [36] carried out fretting and plain fatigue tests using Inconel 100 specimens and obtained an increase of the fatigue strength at 600◦C under fretting fatigue conditions. Attia [32] compared the decrease in the fatigue strength of Inconel 600 and Incoloy 800 between fretting and plain fatigue tests in the steam environment at 265C. Attia observed a reduction factor from 2.5 to 3.5 in the fatigue strength due to fretting. Fellows et al. [31] carried out several fretting fatigue and plain fatigue tests of Inconel 718 specimens. After applying a fracture mechanics-based approach concluded that Inconel 718 has a significant resistance to crack initiation under fretting fatigue conditions. However, the authors pointed out that Inconel 718 showed elevated strength to fretting conditions, being almost insensitive when comparing with plain fatigue results. An interesting result was found by Lee et al. [30] when studying the crack initiation and propagation under fretting conditions of Inconel 600 alloy. They observed that the crack growth rates were greater in plain fatigue than fretting fatigue conditions. The reason was the introduction of the debris generated due to fretting between the contacting bodies in the micro-cracks and, thus, modifying the crack closure. On the other hand, wire electrical discharge machining (WEDM) is another alternative when manufacturing Inconel 718. Up to date, there is no information regarding the influence of WEDM in the Inconel 718 fretting fatigue behaviour. However, some authors have demonstrated that the fatigue strength of Inconel 718 WEDM manufactured specimens is reduced from 10 to 30% in comparison with a polished sample [36].

Some of the machining factors that may affect the SI are the cutting speed, depth of cut, feed rate, coolant conditions, cutting tool geometry, cutting tool material and cutting tool state (worn or new). These aspects are usually dependent on each other. For instance, cutting speed strongly influences the evolution of the cutting tool state and, thus, modifies the cutting tool geometry. The literature about the influence of different machining factors on the SI of Inconel 718 is vast. It is not our intention to perform a thorough review of the current machining Inconel 718 technologies and the reader is referred to the extensive work in the literature (i.e., [37,38]) for further details of the state of the art.

Carbide and ceramic tools are commonly used in finishing operations, however recent developments of new PCBN materials with higher resistance and strength at high temperatures have allowed to implement high-speed machining of hard-to-cut materials such as Inconel 718. Some authors have demonstrated that machining Inconel 718 with PCBN tools at high speed can introduce residual compressive stress at the machined surface [39–43]. However, other aspects of the SI may change during the introduction of compressive residual stress such as the microstructure or surface finish introduction and, thus, decreasing the fatigue strength.

This work analyses the influence of different machining parameters using carbide and PCBN cutting tools, in the fretting fatigue behaviour of Inconel 718. The development of a specific fretting fatigue test rig and the experimental set-up is described. The methods applied to manufacture the samples as well as the techniques and measurements used to characterise its SI are presented. Finally, the trends observed on fretting fatigue lives until complete fracture and a discussion of the experimental results are presented.

2. Materials and methods

2.1 Material: Inconel 718

The alloy Inconel 718 used in the experiments was hardened by solution heat treatment and aged. The material was heat up to 980ºC for 90 minutes and water quenched. The material was subsequently heated at 720ºC for 7 hours and decreased the temperature to 56ºC/h until reaching 621ºC that was kept for 8 hours, and finally air quenched. The material treatment was similar to that typically presented during finishing operations in industrial applications. The chemical composition of the alloy is shown in Table 1.

Element	Ni	Cr	Fe	Nb	Mo	Ti	Al	Co	Si	Cu	Mn	C
%	53.02	18.49	18.12	5.4	3.06	0.96	0.55	0.1	0.06	0.05	0.06	0.03

Table 1: Element composition of alloy 718.

Uniaxial tensile tests were carried out in the specimen until complete fracture in order to characterise the material stress-strain behaviour. Testing was performed in a hydraulic press machine Instron 8801 with a load cell suitable for maximum load of 100 kN. Table 2 presents a summary of the main material mechanical properties obtained from uniaxial testing.

Young's modulus	E	205 GPa
Yield stress	σ_y	1025 MPa
Ultimate stress	σ_u	1375 MPa
Fatigue limit [10^6] (R=-1)	S_N	500 MPa [35]
Fatigue strength coefficient	σ_f'	5964.86 MPa [35]
Fatigue strength exponent	b	-0.166 [35]

Table 2: Mechanical and fatigue properties of Inconel 718.

2.2 Specimen preparation

The starting material was a hollow cylinder with internal diameter 40 mm, external diameter 152 mm and 60 mm length. First of all, the round bar was cut into discs of 10 mm thickness using wire electrical discharge machining (WEDM). Next, both sides of each disc were faced in a Pinacho Smart Turn 6/165 CNC lathe, reducing the disc thickness to 8 mm. The depth of cut and feed rate was fixed to 0.15 mm and 0.15 mm/rev, respectively, in all machining operations. However, the cutting tool, coolant pressure and tool state used for machining each disc were changed, resulting in different machining parameter combinations. Furthermore, two cutting speeds were used for each disc. In each disc, the outer half of the semi-disc was machined at high cutting speed and the other half at low cutting speed. Lastly, WEDM was used to cut out the silhouette of the dog bone specimens. Figure 1 shows a sketch of the followed operations to obtain the dog-bone shape specimens explained above.

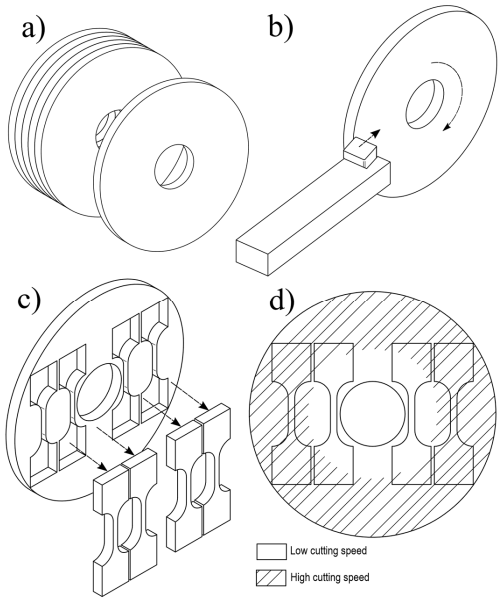

Figure 1: Sketch of the manufacturing procedure to obtain the dog-bone specimens (subfigures a, b and c) and top view of the discs showing the machined surfaces at high and low cutting speed (subfigure d).

As a result, 12 different machining conditions were tested and two specimens were obtained per condition. Table 3 details the 12 machining conditions defined with its corresponding test code denoting the specimens. In this way, two cutting tools at high and low cutting speed were used (the cutting speed values were adjusted to the current speed ranges recommended by the tool manufacturer): a carbide tool at 50 and 70 m/min and a PCBN tool at 200 and 300 m/min, respectively. The cutting conditions were defined from previous investigations based on optimum tool performance in terms of tool efficiency [44,45]. A water-soluble cutting fluid was employed at a pressure of 7.5 bar using an external cooling system through the tool holder and applied at the cutting zone. In addition, the PCBN tool has also been used with a high coolant pressure of 70 bar. The high coolant pressure was not applied in the carbide tool because its influence on medium or lower cutting speeds, such as in carbide tools, is usually not relevant [46]. Lastly, all the previous machining conditions were performed at two different tool initial wear levels, when the tool is completely new and at the end of its life when it is considered worn. The tool criteria defined for the end of life is 0.4 mm of flank wear which is a common criterion for tool replacement in industry.

Test code	Cutting insert	Cutting speed [m/min]	Tool state	Coolant pressure [bar]
NCARB_S050_LP	Carbide	50	New	7.5
WCARB_S050_LP	Carbide	50	Worn	7.5
NCARB_S070_LP	Carbide	70	New	7.5
WCARB_S070_LP	Carbide	70	Worn	7.5
NPCBN_S200_LP	PCBN	200	New	7.5
WPCBN_S200_LP	PCBN	200	Worn	7.5
NPCBN_S300_LP	PCBN	300	New	7.5
WPCBN_S300_LP	PCBN	300	Worn	7.5
NPCBN_S200_HP	PCBN	200	New	70
WPCBN_S200_HP	PCBN	200	Worn	70
NPCBN_S300_HP	PCBN	300	New	70
WPCBN_S300_HP	PCBN	300	Worn	70

Table 3: Test matrix of the different machining conditions studied.

The cutting inserts used in this work were provided by Seco. Both tools are usually recommended for industrial application in finishing operations of nickel-based alloys. On the one hand, a carbide tool TS2000 grade with TiN+TiAlN coating, a nose radius of 0.4 mm. On the other hand, a PCBN tool grade CBN170 with low CBN content (60%), a ceramic binder, a nose radius of 0.8 mm and without coating. The cutting-edge preparation of both tools is a round honing with a nominal radius of 25 microns. The carbide insert was assembled on a tool holder 2525M09JET with the following cutting angles: 17° of rake angle and 7°of clearance angle. The PCBN insert was assembled on a tool holder PCLNR2525M12 with the following cutting angles: -6°of rake angle and 6° of clearance angle. The cutting geometries are different because PCBN tools are not able to cut at large rake angles. The main reason is because PCBN material is harder than carbide, but less tough. Therefore, it requires a cutting geometry that improves its strength against a brittle failure such as negative rake angles.

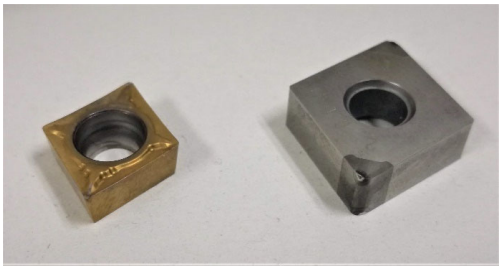

Figure 2: Picture of the carbide tool (left) and PCBN tool (right).

2.3 Surface integrity characterisation

Machining induced surface residual stresses and surface roughness were measured in all specimens. Because of the characteristic waviness shape of the surface after turning, measurements were taken in two orthogonal directions: parallel (0°) and perpendicular (90°) to the longitudinal axis of the dog-bone specimens. Surface roughness was measured using a surface roughness tester Mitutoyo model SJ-201 (Mitutoyo, Tokyo, Japan). Three measures of the arithmetical mean deviation of R_a were taken for each direction. In addition, two measures of the residual stresses at the surface in each direction were taken using X-ray diffraction by IK4 Ideko. The following parameters characterised for the measurement of the RS: 40 s of exposure time, 30 kV of X-ray voltage, 6.7 mA of X-ray current, CrKα tube and 2 mm diameter of the collimator.

2.3 Experimental fretting fatigue set-up

Dovetail joints in the blade/disk assembly in turbines are usually made of alloy 718. The contact type which better reproduces the stress state in a real component is a flat pad with rounded edges clamped to a flat surface as it is demonstrated in [47]. Therefore, a flat pad with rounded edges was selected to perform the fretting fatigue tests. Pads were made from the same discs of alloy 718 used for the manufacturing of the specimens. Pads were manufactured by WEDM. Figure 3 shows the principal dimensions and shape of both pads.

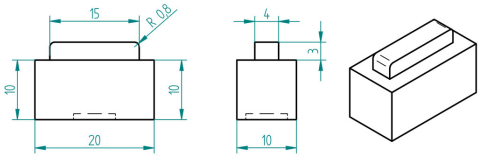

Figure 3: Sketch of the pad geometry with a rounded edge of 0.8 mm.

The experimental set-up was carefully designed to ensure the test repeatability and to control some of the most relevant fretting parameters. The fretting fatigue fixture used in the experimental set-up is shown in Figure 4. Normal loading is symmetrically applied on two pads, one on each side of the specimen, using a proving ring with two screws. A strain gauge is attached on the surface of the

proving ring to measure the normal load. The calibration of the proving ring was performed in the same machine where the fatigue tests are conducted.

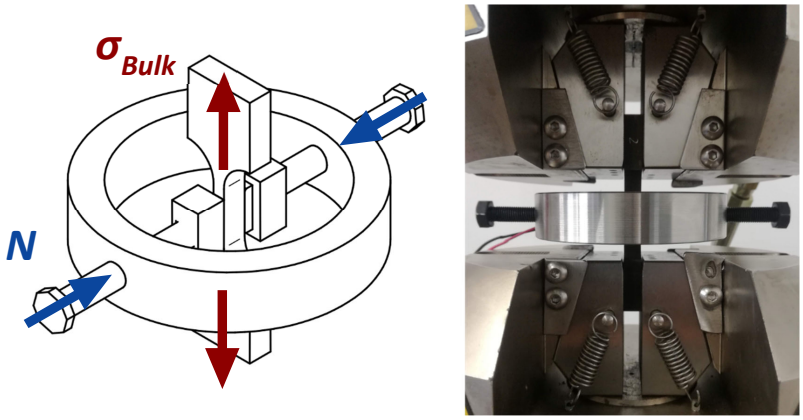

Figure 4: Sketch and picture of the experimental fretting fatigue experimental test set-up.

A specific tool with the geometry of the final assembly was developed to ensure the alignment and correct location of the pads with respect to the specimens (see Figure 5) during the application of the normal load. Next, the specimen is placed on an Instron 8801 fatigue testing machine, for further cyclic bulk loading with a sinusoidal waveform. All the fatigue tests were conducted under force control with a frequency of 10 Hz.

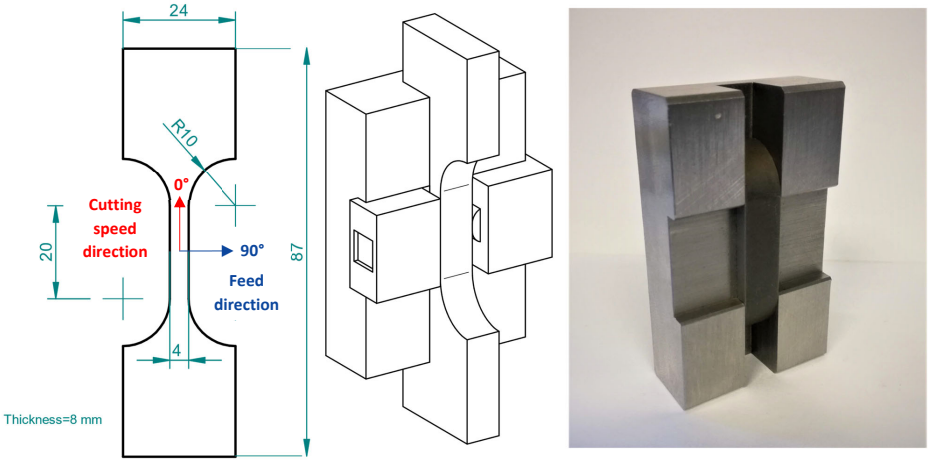

Figure 5: From left to right: sketch with specimen dimensions, sketch of the assembly with the specimen, pads, and alignment tool during application of normal load and picture of the alignment tool.

In this fretting fatigue test configuration, the proving ring is floating, the acting forces are the normal load, the friction force, and the gravitational force which is negligible in comparison with the other forces involved. Therefore, a tangential force is not developed during the test, although friction tractions along the contact zone arise due to the elongation of the specimen. Due to equilibrium, these friction tractions are self-balanced with respect to the centre of the contact [48].

All the specimens were tested under identical testing conditions. During the test execution, some specimens of Inconel 718 failed due to plain fatigue. In these tests, the fracture occurred at the stress raiser near the neck of the dog-bone specimen. Therefore, we applied a pre-load of 950 MPa in all the Inconel 718 samples in order to take advantage of the plasticity properties of the material to introduce compressive RS at the stress raiser near neck of the specimens. Thus, increasing the fatigue strength locally at the neck of the specimen. The load is set in order to do not exceed the yield stress at the centre of the section where the cross-section is constant and where the fretting pads are placed. The normal load applied on the fretting ring was 50 MPa (2.68 kN) and the maximum bulk load was 400 MPa (12.8 kN) using a stress ratio equal to -1.

3. Results

The slip amplitude calculated considering full sliding on the contact edge corners is 13.4 μm. Under these circumstances of small slip amplitude and partial-slip conditions, wear is usually negligible [13]. However, it was enough to damage the surface of the pads (see Figure 6) specially affecting the region close to the rounded edges where some material was transferred to the dog-bone samples.

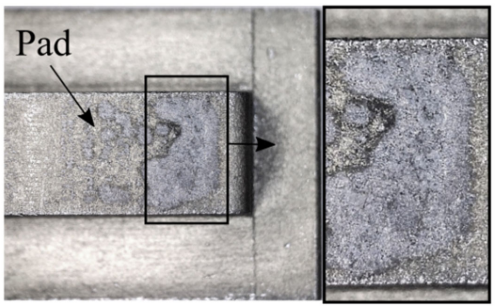

Figure 6: Optical microscope image of a fretting scar on a flat pad with rounded edges (PADR0.8) for the test in an Inconel 718 belonging to the main set.

In most cases, specimen failure was due to a crack initiated along the edge of the contact area that propagated until the complete fracture of the specimen as in the previous experiments. Multiple non-propagating micro-cracks were also observed close to the fretting edge beneath the contact (see Figure 7). In general, the dominant crack was located just at the edge of the contact. Although the four contact edges were susceptible to develop a crack, only one developed macro-crack as it was observed in all the tests conducted. However, some specimens failed prematurely due to a crack initiated at the neck of the dog-bone specimen because of the
stress raiser produced by the change of section.

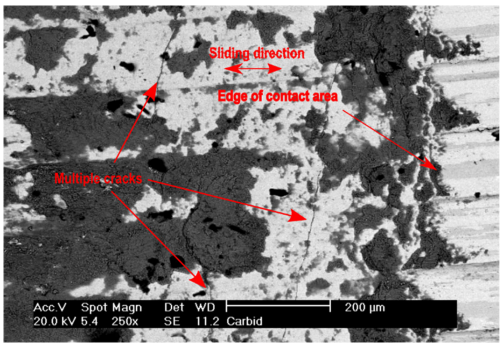

Figure 7: SEM image of a fretting scar of test NCARB_S050_LP.

Figure 8 shows two pictures taken by SEM of half of the fretting scars obtained for tests NCARB_S050_LP (left) and NPCBN_S200_LP (right). The fretting scars were quite similar to those obtained for the specimens of the trial set. Some adhesion of the debris generated during the test is observed close to the edge of contact. In this case, the debris was preferentially adhered to the valleys of the waviness surface obtained after turning with the carbide tool.

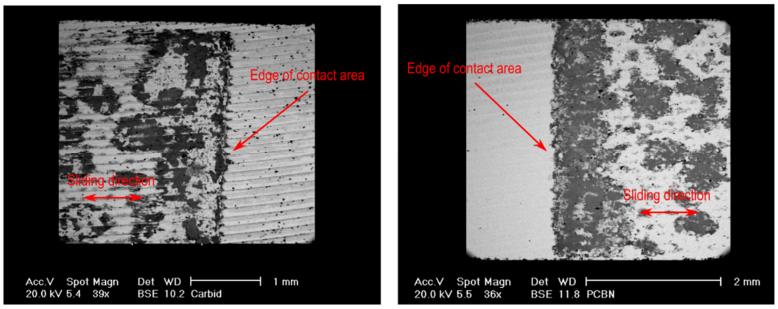

Figure 8: SEM image with low magnification of a fretting scar for the test NCARB_S050_LP (left) and NPCBN_S200_LP (center).

Figure 9 shows the fracture surface for the test condition NPCBN_S300_LP. Multiple cracks initiate along the contact edge. In most cases, cracks were initiated at the zone beneath the contact. As it can be seen, part of the debris is trapped and adhered to the fractured surface close to the crack initiation area. Lastly, Figure 9 shows a very large fatigue crack growth fracture section higher than 80% of the global cross section, showing the high fracture toughness of the material.

Comentado [HM1]: Esto no se ve, si quieres mete un aumento de imagen de la zona de iniciación, con más aumentos

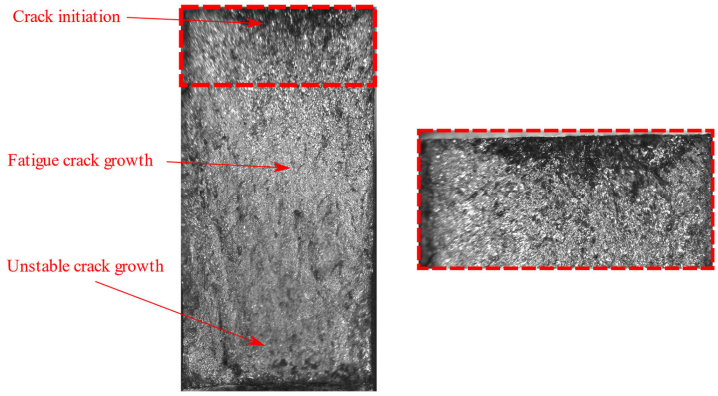

Figure 9: Fracture surface of a broken dog-bone specimen of test condition NCARB_S050_LP.

3.1 Surface integrity results

The tool type, cutting speed and tool state are the factors analysed. Each factor has two levels: PCBN or carbide tool, high or low cutting speed and new or worn tool. Table 4 lists the mean surface roughness and surface residual stresses of the measurements performed in two orthogonal directions

for all tested conditions. As it can be seen, the best mean surface finish in terms of surface roughness was found for test condition WPCBN_S300_LP in 0º and 90º with a value of 0.11 µm and 0.35 µm, respectively. On the other hand, the worst surface finish was found for test NCARB_S050_LP and NCARB_S070_LP with a result of 0.66 µm and 1.39 µm, respectively. The mean value for the surface roughness at 0º was 0.31 µm and 0.84 µm for the orthogonal direction. In terms of surface residual stresses, the higher compressive residual stress mean value was found for the machining condition used in test WCARB_S070_LP with a value of -232.55 MPa for 0º direction. On the other hand, only tensile residual stresses were found for the 90º direction with a maximum value of 1253.05 for test WPCBN_S300_LP and a minimum of 366.50 for test NCARB_S050_LP. The mean residual stresses of all tested conditions measured at 0º and 90º were 329.73 MPa and 814.50 MPa, respectively. Note that the fatigue loading direction is defined in the 0º direction. Thus, it is expected that surface integrity results related the loading direction may have a larger impact on the fatigue behaviour.

Coolant pressure [bar]	Cutting insert	Cutting speed [m/min]	Tool state	Test code	R_a [µm]		RS [MPa]	
					0º	90º	0º	90º
7.5	Carbide	50	New	NCARB_S050_LP	0.66	1.36	403.40	366.50
			Worn	WCARB_S050_LP	0.45	1.10	-68.45	478.95
		70	New	NCARB_S070_LP	0.43	1.39	337.70	468.05
			Worn	WCARB_S070_LP	0.17	0.57	-232.55	728.55
	PCBN	200	New	NPCBN_S200_LP	0.30	0.82	589.05	795.15
			Worn	WPCBN_S200_LP	0.29	1.14	458.85	1196.40
		300	New	NPCBN_S300_LP	0.16	0.69	337.90	760.95
			Worn	WPCBN_S300_LP	0.11	0.35	528.00	1253.05
70		200	New	NPCBN_S200_HP	0.44	0.77	607.85	678.55
			Worn	WPCBN_S200_HP	0.26	0.53	269.70	1005.90
		300	New	NPCBN_S300_HP	0.28	0.81	748.70	1144.40
			Worn	WPCBN_S300_HP	0.16	0.55	-23.45	897.55

Table 4: Mean results for surface roughness and residual stresses for all tested conditions in two orthogonal directions measured on the specimen surface.

In order to assess the effect of the machining parameters, surface integrity measurements are divided into two different sets of data for each factor studied (i.e., tests performed using a carbide or a PCBN tool) and for each surface integrity variable analysed (R_a at 0º and 90º and RS at 0º and 90º). Therefore, a box-and-whisker diagram of the surface roughness and residual stresses measurements for each factor are presented in Figure 10 and Figure 11, respectively. The values presented in these box plots are the median (horizontal black bar inside the box), the first and third quartile (upper and bottom limits of the box) and the minimum and maximum values excluding possible outliers (whiskers). A possible outlier is classically defined as a value exceeding the first and third quartile plus 1.5 times

the interquartile. As it can be seen in Figure 10, the differences between the median values of the surface roughness are not significantly large at 0º. Furthermore, trends observed between levels for each factor are the same for the measurements at 0º and 90º. However, the differences between levels at 90º directions are higher, especially between the data sets corresponding to machining conditions with a carbide tool or a PCBN and when machining with different tool states. This result was expected because the nose geometry of the PCBN tool is twice the size of the carbide tool. In addition, the nose radius usually increases as wear develops being equivalent to machining with a cutting insert with a larger nose radius.

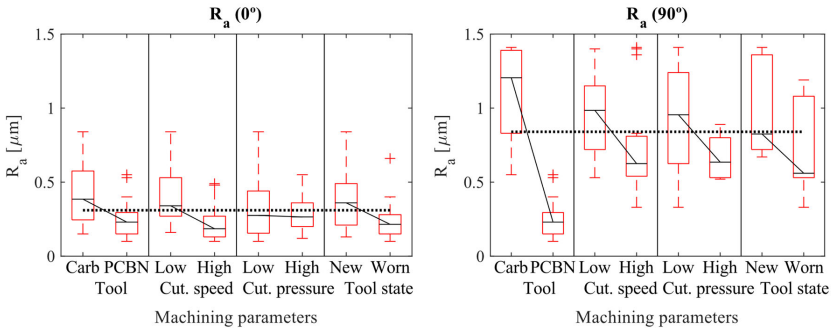

Figure 10 Surface roughness measurements at two orthogonal directions for all machining factors studied expressed in abox-and-whisker plot.

In terms of residual stresses, we can observe that the effect of the cutting speed, and cutting pressure is not very significant. However, the tool state shows a relevant influence on the residual stresses at 0º. Additionally, the observed trend is opposite at 90º, using a worn cutting tool produces compressive residual stresses at 0º, but higher tensile residual stress values at 90º. Lastly, the box plot shows that specimens machined with the carbide tool usually generate lower residual stresses than the PCBN tool for both directions.

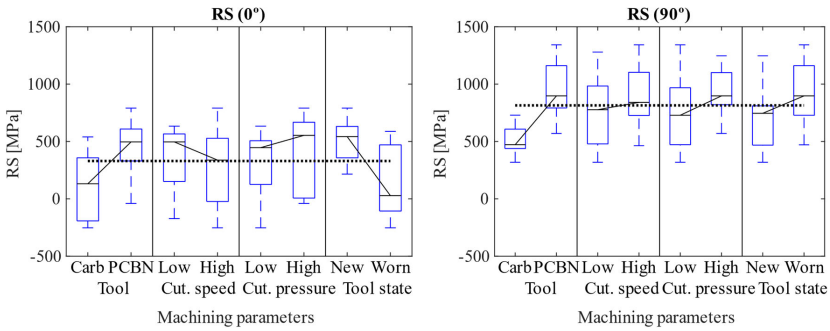

Figure 11: Box-and-whisker plot of surface residual stress measurements at two orthogonal directions for all machining factors studied.

3.2 Fretting fatigue life

Table 5 lists the mean cycles until failure in the fretting fatigue tests performed. The mean life to failure was 2.43E+05 cycles. The longest test took 3.95E+05 cycles (WCARB_S070_LP) and the shortest test lasted 1.31E+05 cycles (NPCBN_S200_HP). The strength-reduction factor (SRF) at 2.43E+04 cycles calculated through Basquin's power-law regressions using the constants listed in Table 2 is 1.69. The value of the SRF is usually around 3 for several engineering alloys [49], although it can be greater than five [50]. In this case, Inconel 718 presents higher fretting fatigue strength than common alloys, suitable forcomponents under fretting conditions. In addition, the SRF of Inconel 718 obtained in this work is close to the value obtained by Hamdy and Waterhouse [201], differences about 25% could be related to variations in the workpiece material and testing conditions. Note that only one test was considered for test conditions NCARB_S070_LP and NPCBN_S300_HP because they failed prematurely due to plain fatigue conditions.

Test code	N_f [cycles*10^5]
NCARB_S050_LP	1.31
WCARB_S050_LP	3.54
NCARB_S070_LP	1.73
WCARB_S070_LP	3.95
NPCBN_S200_LP	2.39
WPCBN_S200_LP	2.33
NPCBN_S300_LP	1.59
WPCBN_S300_LP	2.08
NPCBN_S200_HP	2.15
WPCBN_S200_HP	2.88
NPCBN_S300_HP	2.22

WPCBN_S300_HP	3.02	

Table 5: Mean fretting fatigue cycles to failure for the specimens belonging to the main set machined under LPC.

Analogously to the surface integrity section, a box plot diagram is presented in Figure 12 with the results of the fretting fatigue lifetime until complete fracture. The results show that the tool state has the most statistical significance effect, followed by the cutting fluid pressure. However, a large scatter of the total lifetime is presented when using a worn tool with cutting pressure of 7.5 bar. On the other hand, the cutting speed and type of tool possess a weak relevant effect on the cycles until complete fracture.

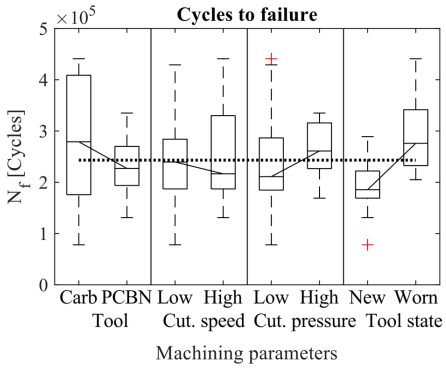

Figure 12: Box-and-whisker plot of the mean fatigue cycles until fracture data sets associated with each level and machining factor.

4. Discussion

In all cases analysed, the observation of the fretting scars under optical microscopy has revealed that some material from the pad surfaces was transferred and adhered to the plane specimen surfaces. This phenomenon was mainly caused because pads were manufactured by WEDM. Although WEDM is an appropriate technique to achieve complex silhouettes like the pad geometries, surface may be altered such as hardness, in comparison to bulk material, that is prone to be removed as debris or adhered to the flat surfaces during the fretting fatigue tests. No significant differences were found in the fretting scars observed between specimens made of Inconel 718. Some debris generated during the tests from the pad surface was usually transferred to the specimen, especially close to the contact edges where the higher slip amplitudes are expected to occur. The peaks of the waviness shape

produced by the turning operations were almost removed or closed up in fretting zones as shown in Figure 7. Therefore, the effect of the surface topography (i.e., the surface roughness) may play a role at the beginning of the test, but not after running enough cycles until wear removes it. As shown in the fractured surfaces (see Figure 9), part of the generated debris is adhered also to the crack surfaces close to the crack initiation area. This debris trapped in the generated micro-cracks may influence the crack closure behaviour as demonstrated previously in [30]. Another point to consider is the vertical position of the specimens during testing. Thus, debris developed at the bottom contact edges is more prone to escape from the contact due to gravity forces than the debris generated at the upper edges. However, the side of failure appeared indistinctly at the bottom or upper edges.

For proper discussion of the results, two figures are included in this section regarding the surface roughness measures. Figure 13 shows the mean fatigue lives using bars and the surface roughness R_a for all the machined conditions. As commented above, surface measures were taken in two directions: parallel (0º) and perpendicular (90º) to the longitudinal axis of the fatigue load. Note that 0º direction (longitudinal axis of the specimen) is parallel to the cyclic axial load and fretting movement direction. Furthermore, the fretting movement direction is almost parallel to the cutting force component during machining in Figure 5. In the case of new tools, the measures obtained in the R_a are in line with the results obtained by Arunachalam et al. [41] for carbide tools. Considering the effect of tool wear, the surface roughness decreases as the flank wear increases in agreement with Díaz-Alvarez et al. [45]. When the tool is new, the cutting tool has a sharper edge. The progression of tool wear (flank wear mainly in this case) increases the deformation at the machined surface resulting in decreased roughness as has been observed by other authors [45,51]. It is well known that surface finish has a huge impact on the fatigue performance, especially for small loads where the crack initiation time dominates the fatigue life. However, previous studies have reported that the effect of surface roughness on fretting fatigue is not as relevant as in plain fatigue conditions [15,17]. In this work, the variation in the mean values obtained when comparing different tests, particularly in the 0º direction, seems to be negligible, especially if we compare the values with the estimated slip amplitude, whose value is close to 13.4 μm. However, it should be considered in Figure 13 that the longest test condition was obtained when surface roughness was 0.17 μm (close to the minimum surface roughness obtained) at 0º and the shortest test when surface roughness was maximum at a value of 0.66 μm.

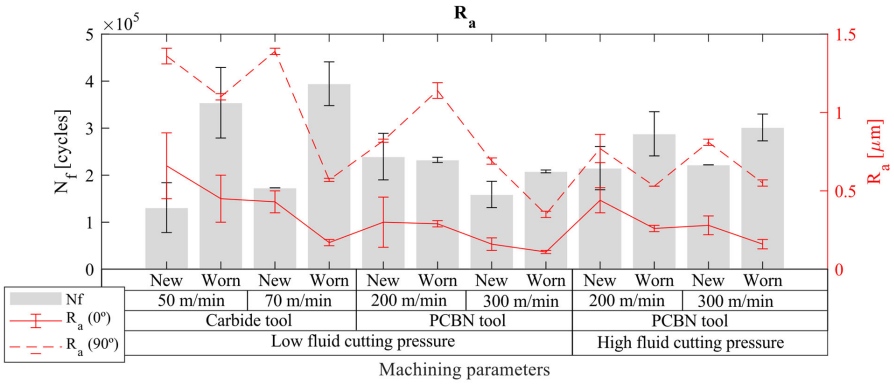

Figure 13: Cycles to failure (bars) and surface roughness (solid and dashed line) measured in two orthogonal directions.

Figure 14 shows together the fatigue lives using bars and the RS at the surface for all cases analysed. Mostly tensile RS were obtained in all cases, slightly better performance has been observed when using a worn carbide tool, leaving lower surface tensile stresses or even compressive stresses in the 0º direction. In addition, the results obtained using a worn PCBN tool and high-pressure coolant have generated compressive RS, but with higher scattering of the results. RS in machining is due to competition of plastic deformation produced by mechanical loads, thermal effects and material volume changes induced by metallurgical alterations [52]. In general, plastic deformation induced by mechanical loads produces compressive RS, meanwhile, thermal effects produced by local heating produced during machining may be responsible for shifting the RS towards tensile [52,53]. Thus, a possible explanation for these results is a change in the dominant mechanism of residual stresses formation between the thermal effects and the higher mechanical loads produced by the flank wear developed in the worn cutting tools that changes the cutting geometry compared to the fresh or new tool [43], especially when using high-pressure coolant. Note that Inconel 718 experiences extreme work hardening and the machining forces can increase up to 5-8 times their initial values as tool wear progresses [45]. It is difficult to compare the results to other studies since test conditions are different in terms of tool material or cutting geometries. Furthermore, there is some controversy in the literature regarding the influence of the tool wear on the RS [7,40,43,54,55]. However, most trends observed in this work are in line with previous studies found in the literature [7,55]. In particular in the 0º direction, the residual stresses are lower when using worn tool with flank wear. This trend was also observed by Madariaga et al. [7]. In addition, the 0º direction is more critical than the feed direction on the fretting fatigue performance because it is directly related to the fretting fatigue load direction and, thus, to the crack opening. However, if the axial fatigue load would have oriented to the feed

direction, the fatigue results would have been significantly affected since the trend observed in the feed direction residual stresses (90º) is just the opposite of the trend observed in the cutting direction. This result shows the huge effect of the machining orientation of the samples in the SI of the specimens obtained.

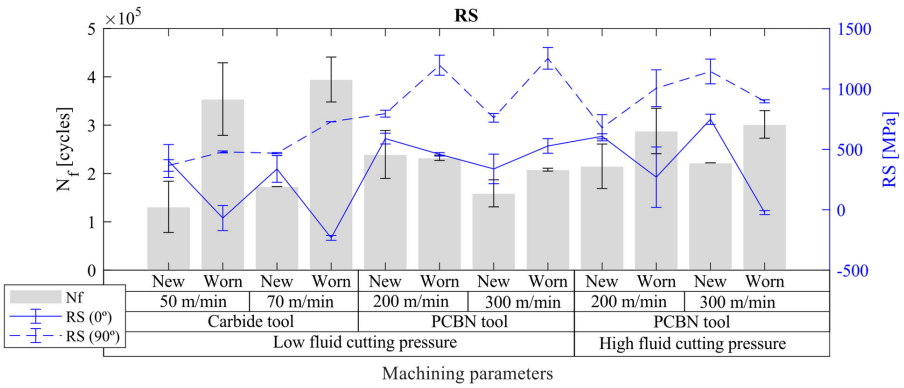

Figure 14: Cycles to failure (bars) and surface residual stresses (solid and dashed line) measured in two orthogonal directions.

The relationships between the SI mean measures, R_a and RS, and the fretting fatigue lives are summarized in Figure 15. Furthermore, the function obtained for each variable of a linear regression analysis and the correlation factor are also presented in the same figure. The measures obtained in the 90º orientation showed a poor linear correlation in comparison with the results obtained with the 0º orientation. It is observed a clear relationship between the residual stresses measured in the 0º direction (see also Figure 14) and the lives obtained in the fretting fatigue tests. In this case, the correlation factor is not large enough to establish a linear relationship since the fretting fatigue performance is a complex phenomenon depending on many other factors, such as metallurgical alterations. However, the surface residual stress in the loading axis direction has shown to be a good indicator for the fretting fatigue and machining performance. On the other hand, considering the results obtained in this work, there is a weaker relationship between the surface roughness and the fretting fatigue lives.

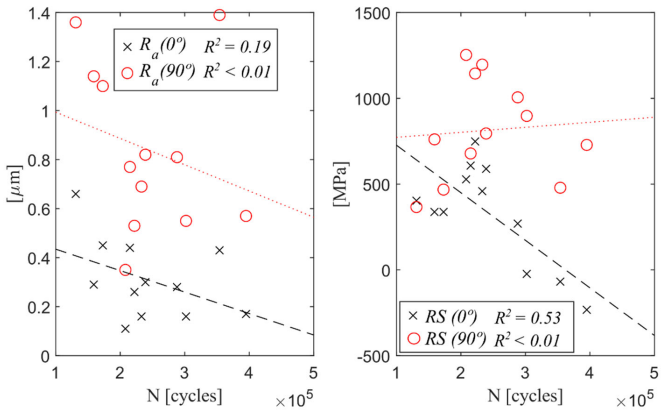

Figure 15: Cycles to failure vs mean surface roughness values (left) and cycles to failure vs mean RS values (right) for all test conditions.

In case of using a linear regression model to model the experimental cycles until failure with RS and R_a measurements at 0º direction, the *R*-square value increases up to 0.65. Figure 16 shows the correlation obtained by the linear regression model explained above.

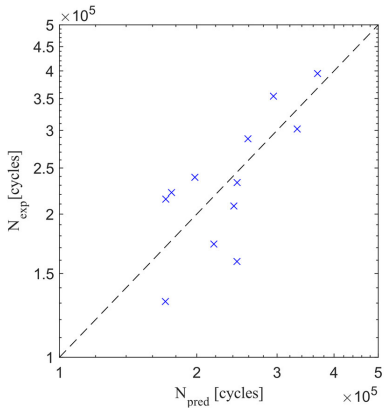

Figure 16: Correlation between experimental cycles until failure and predicted results using a linear regression model using R_a (0º) and RS (0º) as variables.

5. Conclusions

In general, this work analyses the effect of the machining parameters in the fretting fatigue behaviour of specimens made by a hard-to-cut metal, Inconel 718. Due to the lack of experimental results regarding fretting fatigue of Inconel 718, this work provides valuable information regarding surface

integrity and fretting fatigue behaviour using a common contact configuration used in real application such as in dovetail joints for different machining conditions.

The main conclusions of this work are listed below:

- The most significant parameter analysed influencing the fretting fatigue lives was the tool state and the type of tool.
- A slightly better performance was produced when using worn tools in terms of fretting fatigue lives and compressive residual stresses in the 0º direction, but a mean worse performance in the 90º direction was observed.
- In general, the carbide tool showed better surface integrity results than the PCBN tool, except with the PCBN at high cutting speed and high coolant pressure.
- It has been shown that residual stresses play a more significant role than surface roughness in fretting fatigue tests.
- In some cases, it has been observed compressive residual stresses when machining with worn tools which have resulted in longer fretting fatigue lives. However, it should be noted that the use of a worn tool increases the probability to leave notches and defects in the machined surface. In fretting fatigue tests, the possibility that a surface defect is located inside the crack initiation region is lower because the crack initiation area is concentrated in a small region of the specimen and, thus, decreases its influence.

Further work related to the study of the influence of tool wear and end-of-life criteria of cutting tools on the SI and in-service behaviour is required for a better understanding and optimisation of the machining processes. Lastly, possible future research could be related to the extension of this study to other machining operations, such as milling, since the results obtained in this work are limited to the facing operation.

Acknowledgments

The authors gratefully acknowledges the work:

- Proyecto coordinado nuevo amos subproyectos
- prometeo

TO BE WRITTEN

References

[1] R.C. Reed, The Superalloys fundamentals and applications, Cambridge University Press, 2006. https://doi.org/10.1017/CBO9780511541285.

[2] R.E. Schafrik, D.D. Ward, J.R. Groh., Application of alloy 718 in GE aircraft engines: past, present and next five years, Superalloys. 625 (2001) 1–11.

[3] D. Ulutan, T. Ozel, Machining induced surface integrity in titanium and nickel alloys: A review, Int. J. Mach. Tools Manuf. 51 (2011) 250–280. https://doi.org/10.1016/j.ijmachtools.2010.11.003.

[4] J. Holmberg, A. Wretland, P. Hammersberg, J. Berglund, A. Suárez, T. Beno, Surface integrity investigations for prediction of fatigue properties after machining of alloy 718, Int. J. Fatigue. 144 (2021) 106059. https://doi.org/10.1016/J.IJFATIGUE.2020.106059.

[5] T. Klotz, H.Y. Miao, C. Bianchetti, M. Lévesque, M. Brochu, Analytical fatigue life prediction of shot peened Inconel 718, Int. J. Fatigue. 113 (2018) 204–221. https://doi.org/10.1016/J.IJFATIGUE.2018.04.011.

[6] T. Klotz, D. Delbergue, P. Bocher, M. Lévesque, M. Brochu, Surface characteristics and fatigue behavior of shot peened Inconel 718, Int. J. Fatigue. 110 (2018) 10–21. https://doi.org/10.1016/J.IJFATIGUE.2018.01.005.

[7] A. Madariaga, A. Kortabarria, E. Hormaetxe, A. Garay, P.J. Arrazola, Influence of Tool Wear on Residual Stresses When Turning Inconel 718, Procedia CIRP. 45 (2016) 267–270. https://doi.org/10.1016/J.PROCIR.2016.02.359.

[8] I. Ayesta, B. Izquierdo, O. Flaño, J.A. Sánchez, J. Albizuri, R. Avilés, Influence of the WEDM process on the fatigue behavior of Inconel® 718, Int. J. Fatigue. 92 (2016) 220–233. https://doi.org/10.1016/J.IJFATIGUE.2016.07.011.

[9] X. Wang, C. Huang, B. Zou, G. Liu, H. Zhu, J. Wang, Experimental study of surface integrity and fatigue life in the face milling of Inconel 718, Front. Mech. Eng. 13 (2018) 243–250. https://doi.org/10.1007/S11465-018-0479-9.

[10] Y. Lindblom, G. Burman, FATIGUE FAILURE UNDER FRETTING CONDITIONS Yngve Lindblom and Gunnnar Burman FFV Maintenance Division, SWEDEN, (1982).

[11] S.J. Findlay, N.D. Harrison, Why aircraft fail, Mater. Today. 5 (2002) 18–25. https://doi.org/10.1016/S1369-7021(02)01138-0.

[12] D.A. (David A. Hills, D. Nowell, Mechanics of fretting fatigue, Kluwer Academic Publishers, 1994. https://books.google.es/books/about/Mechanics_of_Fretting_Fatigue.html?id=t9Q60-N-13MC&printsec=frontcover&source=kp_read_button&redir_esc=y#v=onepage&q&f=false (accessed July 17, 2019).

[13] M.P. Szolwinski, T.N. Farris, Mechanics of fretting fatigue crack formation, Wear. 198 (1996) 93–107. https://doi.org/10.1016/0043-1648(96)06937-2.

[14] S.C. Gordelier, T.C. Chivers, A literature review of palliatives for fretting fatigue, Wear. 56 (1979) 177–190. https://doi.org/10.1016/0043-1648(79)90017-6.

[15] R.B. Waterhouse, a J. Trowsdale, Residual stress and surface roughness in fretting fatigue, J. Phys. D. Appl. Phys. 25 (1992) A236–A239. https://doi.org/10.1088/0022-3727/25/1A/036.

[16] Studies in Fretting Fatigue - R. Bramhall - Google Llibres, (n.d.).

[17] V. Martín, J. Vázquez, C. Navarro, J. Domínguez, Fretting-Fatigue Analysis of Shot-Peened Al 7075-T651 Test Specimens, Met. 2019, Vol. 9, Page 586. 9 (2019) 586. https://doi.org/10.3390/MET9050586.

[18] J. Vázquez, C. Navarro, J. Domínguez, Experimental results in fretting fatigue with shot and laser peened Al 7075-T651 specimens, Int. J. Fatigue. 40 (2012) 143–153. https://doi.org/10.1016/j.ijfatigue.2011.12.014.

[19] J. Takeda, M. Niinomi, T. Akahori, Fretting Fatigue Characteristics with Relating Contact Pressure and Surface Roughness of Highly Workable Titanium Alloy, Ti-4.5Al-3V-2Mo-2Fe, Mater. Trans. 45 (2004) 1586–1593. https://doi.org/10.2320/matertrans.45.1586.

[20] H. Proudhon, S. Fouvry, J.Y. Buffière, A fretting crack initiation prediction taking into account the surface roughness and the crack nucleation process volume, Int. J. Fatigue. 27 (2005) 569–579. https://doi.org/10.1016/j.ijfatigue.2004.09.001.

[21] A.L. Hutson, M. Niinomi, T. Nicholas, D. Eylon, Effect of various surface conditions on fretting fatigue behavior of Ti-6Al-4V, Int. J. Fatigue. 24 (2002) 1223–1234. https://doi.org/10.1016/S0142-1123(02)00050-6.

[22] A. Volchok, G. Halperin, I. Etsion, The effect of surface regular microtopography on fretting fatigue life, Wear. 253 (2002) 509–515. https://doi.org/10.1016/S0043-1648(02)00148-5.

[23] K. Li, X. Fu, R. Li, P. Gai, Z. Li, W. Zhou, G. Chen, Fretting fatigue characteristic of Ti–6Al–4V strengthened by wet peening, Int. J. Fatigue. 85 (2016) 65–69. https://doi.org/10.1016/j.ijfatigue.2015.12.013.

[24] D. Liu, B. Tang, X. Zhu, H. Chen, J. He, J.P. Celis, Improvement of the fretting fatigue and fretting wear of Ti6Al4V by duplex surface modification, Surf. Coatings Technol. 116–119 (1999) 234–238. https://doi.org/10.1016/S0257-8972(99)00279-0.

[25] S. Chakravarty, R.G. Andrews, P. Painaik, A.K. Koul, The Effect of Surface Modification on Fretting Fatigue in Ti Alloy Turbine Components, (1995) 31–35.

[26] X. Zhang, D. Liu, Effect of shot peening on fretting fatigue of Ti811 alloy at elevated temperature, Int. J. Fatigue. 31 (2009) 889–893. https://doi.org/10.1016/j.ijfatigue.2008.10.004.

[27] H. Murthy, G. Mseis, T.N. Farris, Life estimation of Ti-6Al-4V specimens subjected to fretting fatigue and effect of surface treatments, Tribol. Int. 42 (2009) 1304–1315. https://doi.org/10.1016/j.triboint.2009.04.013.

[28] M.C. Gean, N.J. Tate, T.N. Farris, Fretting fatigue of nickel based superalloys at elevated temperature, Collect. Tech. Pap. - AIAA/ASME/ASCE/AHS/ASC Struct. Struct. Dyn. Mater. Conf. (2009) 2626.

[29] S. Mall, J.L. Ng, E. Madhi, R. Neu, K. Wallin, S.R. Thompson, S.W. Dean, Fretting Fatigue Behavior of Shot-Peened Ti-6Al-4V and IN100, J. ASTM Int. 5 (2008) 101587. https://doi.org/10.1520/JAI101587.

[30] C.Y. Lee, H.-K. Jeung, J.-D. Kwon, Fretting fatigue crack initiation and propagation behavior of Inconel 690 alloy †, J. Mech. Sci. Technol. 30 (2016) 4937–4940. https://doi.org/10.1007/s12206-016-1013-9.

[31] L.J. Fellows, D. Nowell, D.A. Hills, ANALYSIS OF CRACK INITIATION AND PROPAGATION IN FRETTING FATIGUE: THE EFFECTIVE INITIAL FLAW SIZE METHODOLOGY, Fatigue Fract. Eng. Mater. Struct. 20 (1997) 61–70. https://doi.org/10.1111/J.1460-2695.1997.TB00402.X.

[32] M. Attia, Fretting Fatigue of Some Nickel-Based Alloys in Steam Environment at 265°C, ASTM Spec. Tech. Publ. (2000) 231–246. https://doi.org/10.1520/STP14732S.

[33] H.K. Jeung, J. Do Kwon, C.Y. Lee, Crack initiation and propagation under fretting fatigue of inconel 600 alloy, J. Mech. Sci. Technol. 29 (2015) 5241–5244. https://doi.org/10.1007/S12206-015-1124-8.

[34] R.B. Waterhouse, Fretting at high temperatures, Tribol. Int. 14 (1981) 203–207. https://doi.org/10.1016/0301-679X(81)90041-4.

[35] Kawagoishi, Chen, Nisitani, Fatigue strength of Inconel 718 at elevated temperatures, Fatigue Fract. Eng. Mater. Struct. 23 (2000) 209–216. https://doi.org/10.1046/J.1460-2695.2000.00263.X.

[36] S. Mall, H.K. Kim, W.J. Porter, J.F. Ownby, A.G. Traylor, High temperature fretting fatigue behavior of IN100, Int. J. Fatigue. 32 (2010) 1289–1298. https://doi.org/10.1016/J.IJFATIGUE.2010.01.012.

[37] A. De Bartolomeis, S.T. Newman, I.S. Jawahir, D. Biermann, A. Shokrani, Future research directions in the machining of Inconel 718, J. Mater. Process. Technol. 297 (2021) 117260.

https://doi.org/10.1016/j.jmatprotec.2021.117260.

[38] Q. Yin, Z. Liu, B. Wang, Q. Song, Y. Cai, Recent progress of machinability and surface integrity for mechanical machining Inconel 718: a review, Int. J. Adv. Manuf. Technol. 109 (2020) 215–245. https://doi.org/10.1007/s00170-020-05665-4.

[39] J. Zhou, V. Bushlya, R.L. Peng, Z. Chen, S. Johansson, J.E. Stahl, Analysis of subsurface microstructure and residual stresses in machined Inconel 718 with PCBN and Al2O3-SiCw tools, Procedia CIRP. 13 (2014) 150–155. https://doi.org/10.1016/j.procir.2014.04.026.

[40] A.R.C. Sharman, J.I. Hughes, K. Ridgway, An analysis of the residual stresses generated in Inconel 718??? when turning, J. Mater. Process. Technol. 173 (2006) 359–367. https://doi.org/10.1016/j.jmatprotec.2005.12.007.

[41] R.M. Arunachalam, M.A. Mannan, A.C. Spowage, Residual stress and surface roughness when facing age hardened Inconel 718 with CBN and ceramic cutting tools, Int. J. Mach. Tools Manuf. 44 (2004) 879–887. https://doi.org/10.1016/j.ijmachtools.2004.02.016.

[42] R.T. Coelho, L.R. Silva, A. Braghini, A.A. Bezerra, Some effects of cutting edge preparation and geometric modifications when turning INCONEL 718™ at high cutting speeds, J. Mater. Process. Technol. 148 (2004) 147–153. https://doi.org/10.1016/j.jmatprotec.2004.02.001.

[43] R.S. Pawade, S.S. Joshi, P.K. Brahmankar, Effect of machining parameters and cutting edge geometry on surface integrity of high-speed turned Inconel 718, Int. J. Mach. Tools Manuf. 48 (2008) 15–28. https://doi.org/10.1016/j.ijmachtools.2007.08.004.

[44] J.L. Cantero, J. Díaz-Álvarez, D. Infante-García, M. Rodríguez, V. Criado, High Speed Finish Turning of Inconel 718 Using PCBN Tools under Dry Conditions, Met. 2018, Vol. 8, Page 192. 8 (2018) 192. https://doi.org/10.3390/MET8030192.

[45] J. Díaz-Álvarez, V. Criado, H. Miguélez, J.L. Cantero, PCBN Performance in High Speed Finishing Turning of Inconel 718, Met. 2018, Vol. 8, Page 582. 8 (2018) 582. https://doi.org/10.3390/MET8080582.

[46] M. Rahman, A. Senthil Kumar, M.R. Choudhury, Identification of Effective Zones for High Pressure Coolant in Milling, CIRP Ann. 49 (2000) 47–52. https://doi.org/10.1016/S0007-8506(07)62893-5.

[47] M. Ciavarella, G. Demelio, A review of analytical aspects of fretting fatigue, with extension to damage parameters, and application to dovetail joints, Int. J. Solids Struct. 38 (2001) 1791–1811. https://doi.org/10.1016/S0020-7683(00)00136-0.

[48] M. Sabsabi, E. Giner, F.J. Fuenmayor, Experimental fatigue testing of a fretting complete contact and numerical life correlation using X-FEM, Int. J. Fatigue. 33 (2011) 811–822. https://doi.org/10.1016/j.ijfatigue.2010.12.012.

[49] T.C. Lindley, Fretting fatigue in engineering alloys, Int. J. Fatigue. 19 (1997) 39–49. https://doi.org/10.1016/S0142-1123(97)00039-X.

[50] R.B. Waterhouse, Fretting fatigue, Int. Mater. Rev. 37 (1992) 77–98. https://doi.org/10.1179/imr.1992.37.1.77.

[51] J.L. Cantero, J. Díaz-Álvarez, M.H. Miguélez, N.C. Marín, Analysis of tool wear patterns in finishing turning of Inconel 718, Wear. 297 (2013) 885–894. https://doi.org/10.1016/J.WEAR.2012.11.004.

[52] M.M. El-Khabeery, M. Fattouh, Residual stress distribution caused by milling, Int. J. Mach. Tools Manuf. 29 (1989) 391–401. https://doi.org/10.1016/0890-6955(89)90008-4.

[53] F. Gunnberg, M. Escursell, M. Jacobson, The influence of cutting parameters on residual stresses and surface topography during hard turning of 18MnCr5 case carburised steel, J. Mater. Process. Technol. 174 (2006) 82–90. https://doi.org/10.1016/J.JMATPROTEC.2005.02.262.

[54] V. Bushlya, J. Zhou, J.E. Ståhl, Effect of Cutting Conditions on Machinability of Superalloy Inconel 718 During High Speed Turning with Coated and Uncoated PCBN Tools, Procedia CIRP. 3 (2012) 370–375. https://doi.org/10.1016/j.procir.2012.07.064.

[55] A. Muñoz-Sánchez, J.A. Canteli, J.L. Cantero, M.H. Miguélez, Numerical analysis of the tool wear effect in the machining induced residual stresses, Simul. Model. Pract. Theory. 19 (2011) 872–886. https://doi.org/10.1016/J.SIMPAT.2010.11.011.